J. Materials, Conc. Struct., Pavements, JSCE, No. 599/V-40, 155-163, 1998 August

MICROMECHANICAL FIBER PULLOUT MODEL FOR STEEL FIBER REINFORCED CONCRETE

Sunaryo SUMITRO[1] and Tatsuya TSUBAKI[2]

[1] Member of JSCE, Dr.Eng., Japan Structural Engineering and Computer Corp.
(Bunkyo-ku, Tokyo 112-0011, Japan)
[2] Member of JSCE, Ph.D., Professor, Dept. of Civil Eng., Yokohama National University
(Hodogaya-ku, Yokohama 240-8501, Japan)

A micromechanical constitutive relationship is presented for the deformational behavior of steel fiber reinforced concrete under uniaxial tension. Its properties are characterized by a nonlinear interface between concrete matrix and fiber. The interface debonding is examined by the stress criterion expressed in terms of the interfacial shear stress. The present model can take into account the shear stiffness and the shear strength of the fiber-matrix interface, the frictional bond stress, the constraint condition of fiber end, and the effect of the inclination of fiber. The validity of the model is confirmed through simulation for the experimental data.

Key Words *: steel fiber reinforced concrete, microstructure, pullout model, constitutive relationship*

1. INTRODUCTION

In a concrete structure with high mechanical performance, the concrete should have high strength and high toughness and ductility. The mechanical behavior of concrete which is a brittle composite material can be improved by adding a certain amount of steel fibers. In a suitable volume concentration of fibers, microcracks formed in the matrix are stabilized because of the bridging effect of fibers.

To obtain a thorough knowledge of the toughening mechanisms of steel fiber reinforced concrete (SFRC) as a composite material that can lead to the development of a new class fiber reinforced concrete structure, and to make fiber reinforced concrete a practical material used in various concrete structures, it is necessary to understand the constitutive relationship of SFRC. These attempts provide a clue to the optimal design of a SFRC structure (see, e.g., Nanakorn et al. [1]).

To study the constitutive mechanical behavior of SFRC, many types of research works have been done. They may be grouped into two categories, i.e., studies on the macroscopic mechanical behavior of SFRC and those on the microscopic mechanical behavior of SFRC.

To investigate the macroscopic mechanical behavior of SFRC, Cho and Kobayashi [2] studied the behavior of SFRC under uniaxial tensile loading, Chern et al. [3] investigated the behavior of SFRC in multiaxial loading, and Banthia et al. [4] did research of SFRC with various randomly distributed deformed steel fibers under impact loading.

The number of studies on the modeling of the macroscopic mechanical behavior of SFRC is limited at present. Based on simplified composite assumptions of steel fiber and concrete matrix components, a constitutive relationship has been proposed by Sumitro and Tsubaki [5] to express experimentally observed macroscopic deformational behavior of SFRC under multiaxial loading satisfactorily. A constitutive model has also been developed by Sumitro and Tsubaki [6] to be able to express the mechanical behavior of SFRC under impact loading.

However, to make the model more accurate for the three-dimensional micromechanical constitutive model, it is necessary to understand the microscopic deformational behavior and reinforcing mechanisms of the steel fiber component in the concrete matrix.

In addition, this kind of investigation will make it possible to predict the pullout behavior of fibers for given material parameters, to design fibers for desired mechanical properties of SFRC, and

to control the tension-softening of SFRC. These points are considered to be important from the engineering point of view for more reasonable design of concrete structures.

The bond between the fiber and the matrix in SFRC is an essential factor to be considered when dealing with modeling of the microscopic mechanical behavior of SFRC. The basic test to observe the fiber-matrix bond parameters is the so-called fiber pullout test in which a number of inclined or aligned fibers are pulled out simultaneously from a block of concrete matrix as performed by Naaman and Shah [7], Ouyang et al. [8] and Tsubaki et al. [9]. The effect of fiber properties on the tensile mechanical properties of SFRC has also been reported by Tsubaki and Sumitro [10].

To have a physically reasonable description of the fiber pullout process with debonding propagation on fiber-matrix interface, it is necessary to identify the correct material parameters. Two methods have been used to identify the bond parameters: the stress approach (see, e.g., Nammur and Naaman [11]) and the fracture mechanics approach (see, e.g., Gao et al. [12]). These two methods have been compared by Stang et al. [13] and examined by Li et al. [14]. On the other hand, a different approach without debonding propagation modeling was proposed by Li et al. [15]

Aiming at characterizing various fiber debonding and pullout properties, in this research, a micromechanical fiber pullout model is proposed. The debonding between fiber and matrix is examined by the stress criterion where the propagation of the debonded fiber-matrix interface is expressed in terms of the interfacial shear stress. The present model enables to take into account the following factors: the shear stiffness of the fiber-matrix interface, the shear bond strength, the effective frictional bond strength, the effective elastic modulus of the fiber after debonding process occurs, the effect of the end constraint condition of fiber, and the effect of the inclination of fiber. Material constants for these factors are estimated from experimental data.

Finally, the model predictions and the experimental data are compared, and the validity of the present model is verified.

2. MICROMECHANICAL MODEL

(1) Basic equations

In the present model, the fiber end condition is newly introduced to take into account various anchorage types of fiber. Some coefficients are introduced to express the effect of fiber surface condition. The influence of the fiber inclination is also considered.

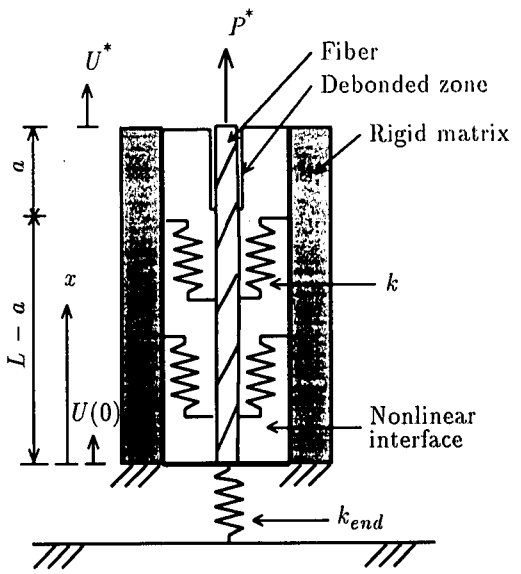

Fig. 1 Fiber model

Fibers inside concrete are modeled by the pullout model using the stress criterion [13]. The pullout model of one fiber is shown in **Fig.1**. A single fiber of a length of L is embedded in a matrix. The matrix is assumed to be rigid except for an interface zone idealized as a nonlinear interface. The shear stiffness of the interface zone of the matrix is k. The end effect of fiber is modeled by a spring with a spring constant k_{end}. The fiber is assumed to have a constant cross-sectional area A_f and an initial elastic modulus E_{f_0}. The effect of Poisson's ratio is neglected for both fiber and matrix.

It is assumed that debonding has occurred over a length a, starting at $x = L$. Assuming that a constant shear stress is acting along the debonded interface [14], it can be written that

$$q = kU(x), \qquad 0 < x < (L-a) \tag{1}$$

$$q = q_f, \qquad (L-a) < x < L \tag{2}$$

where q is the shear force per unit length acting on the fiber. q_f is the frictional shear force per unit length, and $U(x)$ is the fiber displacement. The constitutive relationship for the interface layer is represented in **Fig.2**.

Denoting the fiber force by P, the equilibrium equation is expressed as

$$P_{,x} - q = 0 \tag{3}$$

where a comma preceding a subscript indicates a differential operator, i.e., $(\ )_{,x}$ is the derivative with respect to x. Introducing the constitutive

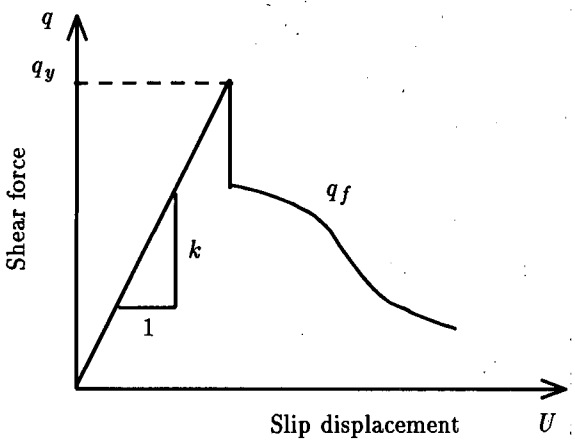

Fig. 2 Constitutive relationship for interface

relationship for the fiber, the following equation is obtained.

$$P = E_f A_f U_{,x} \quad (4)$$

Then, the following differential equations for U are obtained:

$$U_{,xx} - \omega^2 U = 0, \quad 0 < x < (L-a) \quad (5)$$

$$U_{,xx} - \frac{q_f}{E_f A_f} = 0, \quad (L-a) < x < L \quad (6)$$

with a quantity ω defined by

$$\omega = \sqrt{\frac{k}{E_f A_f}} \quad (7)$$

Introducing P^* as the pullout force at $x = L$, the boundary conditions can be prescribed as

$$k_{end}\, U(0) = P(0) \quad (8)$$

$$E_f A_f U_{,x}(L) = P^* \quad (9)$$

The continuity conditions in displacement and fiber load at $x = L - a$ require

$$U(L-a)^- = U(L-a)^+ \quad (10)$$

$$U_{,x}(L-a)^- = U_{,x}(L-a)^+ \quad (11)$$

Solving the above set of equations, the following solutions for the fiber displacement are obtained:

$$U(x) = \frac{P^* - q_f a}{E_f A_f \omega}\left\{\frac{\cosh(\omega x)}{\alpha_1} + \frac{\sinh(\omega x)}{\alpha_2}\right\}, \quad 0 < x < (L-a) \quad (12)$$

$$U(x) = \frac{P^* - q_f a}{E_f A_f \omega}\left\{\frac{\cosh[\omega(L-a)]}{\alpha_1} + \frac{\sinh[\omega(L-a)]}{\alpha_2}\right\} - \frac{q_f}{2E_f A_f}(L-a)^2 - \frac{P - q_f L}{E_f A_f}(L-a) + \frac{q_f}{2E_f A_f}x^2 + \frac{P^* - q_f L}{E_f A_f}x, \quad (L-a) < x < L \quad (13)$$

where

$$\alpha_1 = \sinh[\omega(L-a)] + \frac{k_{end}}{E_f A_f \omega}\cosh[\omega(L-a)] \quad (14)$$

$$\alpha_2 = \sinh[\omega(L-a)]\frac{E_f A_f \omega}{k_{end}} + \cosh[\omega(L-a)] \quad (15)$$

Then, from Eq.(13), the displacement at the fiber end U^* is given by

$$U^* = \frac{P^* - q_f a}{E_f A_f \omega}\left\{\frac{\cosh[\omega(L-a)]}{\alpha_1} + \frac{\sinh[\omega(L-a)]}{\alpha_2}\right\} + \frac{P^* - \frac{1}{2}q_f a}{E_f A_f}a \quad (16)$$

(2) Effective elastic modulus of fiber

The elastic modulus of fiber is reduced by the effect of composite action of fiber and matrix. [5] Therefore, the effective elastic modulus of the fiber E_f is modeled as

$$E_f = a_e E_{f_0} \quad (17)$$

where a_e is a material constant. The coefficient a_e represents the fiber surface condition, i.e., the surface geometry and the bond condition. a_e is different from k which expresses the shear stiffness of the matrix surrounding the fiber, i.e., the interface zone.

(3) Effect of fiber inclination

From the result of tension test on inclined fibers [10], it is assumed that the ratio between the inclined pullout force and the aligned pullout force is proportional to the projection of inclined fiber to the plane that is normal to the crack plane as shown in **Fig.3** and is governed by the following relationship.

$$P^*_\theta = P^*_{\theta=0}\cos(f\,\theta) \quad (18)$$

where P^*_θ is the maximum force for inclined pullout, $P^*_{\theta=0}$ is the maximum force for aligned pullout, and f is the snubbing friction coefficient, i.e., an interface material parameter which can be determined experimentally for each fiber-matrix combination [15]. From the result of the pullout test [10], f is determined as unity in this study.

Then, to model a fiber with an inclining angle θ, the maximum shear force per unit length for inclined pullout $q_{y\theta}$ is assumed to be expressed by

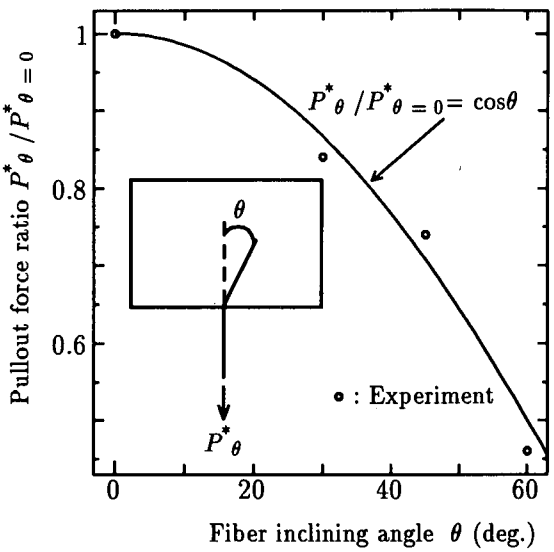

Fig. 3 Relationship between pullout force and inclining angle

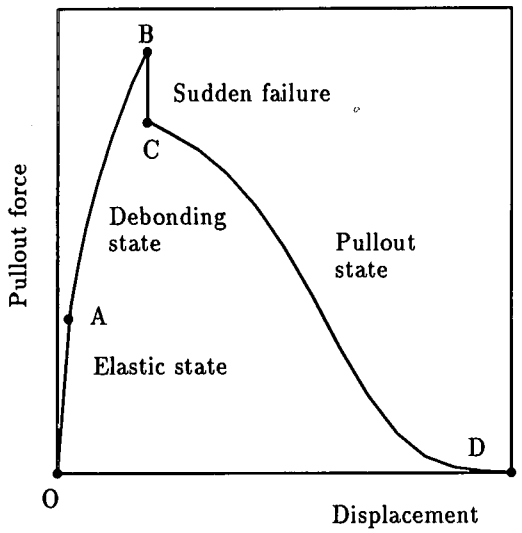

Fig. 4 Schematic load-displacement relationship of a steel fiber

the following relationship in terms of the maximum shear force for aligned pullout $q_{y\theta=0}$.

$$q_{y\theta} = q_{y\theta=0}\cos\theta \tag{19}$$

(4) Effect of fiber end condition

Fibers with various geometrical shapes are used in actual SFRC structures. They can be classified into three kinds, i.e., straight fibers, hooked fibers, and anchored fibers. By considering a different fiber end condition for each fiber type, in this model, it is assumed that the effect of fiber end condition is represented by a spring constant k_{end}.

3. CRITERION OF FIBER PULLOUT

(1) Stress criterion

The stress criterion for debonding is based on the assumption that the debonding takes place only when the maximum shear stress in the interface zone reaches a critical value. The criterion is expressed in terms of shear force per unit length q, and it is assumed that debonding starts when q reaches a critical value q_y.

It is also assumed that q_y is constant, and that the frictional shear force q_f is expressed in terms of the maximum shear force q_y as

$$q_f = D\,q_y \tag{20}$$

where, after debonding occurs, D is assumed to be constant, D_0, up to the peak:

$$D = D_0, \qquad 0 \le D_0 \le 1 \tag{21}$$

The coefficient D expresses the shear transfer capability which depends on the surface condition of the debonded zone.

Then, the solution for q is

$$q = (P^* - Dq_y a)\omega\left\{\frac{\cosh(\omega x)}{\alpha_1} + \frac{\sinh(\omega x)}{\alpha_2}\right\}, \quad 0 < x < (L-a) \tag{22}$$

$$q = Dq_y, \qquad (L-a) < x < L \tag{23}$$

The condition for debonding, $q = q_y$ at $x = L-a$, can be written as

$$P^* = q_f a + \frac{q_y}{\omega}\left\{\frac{\alpha_1\alpha_2}{\alpha_1\sinh[\omega(L-a)] + \alpha_2\cosh[\omega(L-a)]}\right\} \tag{24}$$

(2) Load-displacement relationship

The schematic load-displacement relationship for one fiber is shown in **Fig.4**.

From the origin O to point A, the fiber has an elastic relationship, which is referred to as *elastic state.*

After reaching point A, debonding process starts and propagates up to full debonding that occurs at point B, which is referred to as *debonding state.* During debonding propagation process, the fiber elastic modulus is assumed to be constant for the duration of each load step, having the reduced value.

Either in a displacement-controlled test or load-controlled test, just after reaching point B, a sudden failure occurs and the sustainable load drops to a level at point C. After sudden failure, a successive pullout process continues until the fiber is totally pulled out. This state C–D is referred to as *pullout state*. Assuming that after sudden failure the remaining embedded part of fiber provides frictional resistance, the following relationship holds:

$$P^* = q_f L_f \tag{25}$$

where L_f is the frictional length of fiber. It is assumed that the elongation of the fiber is negligible because it is too small compared to the original fiber length and the total displacement. Thus, the frictional length is considered to be equal to the difference between fiber length and the fiber end displacement as shown in the following equation.

$$L_f = L - U^* \tag{26}$$

In the *pullout state*, it is assumed that D depends on the fiber end displacement as in the following relationship:

$$D = D_0 \exp(-a_d \left[\frac{U^*}{U_0}\right]^{p_d}) \tag{27}$$

where a_d, p_d and U_0 are constants.

Consequently, q_f is not constant in the *pullout state*. This may be attributed to the reduction of shear resistance due to the abrasion of surface roughness of the interface by large slip of fiber.

The exponential function is used for the coefficient D because it can represent wide range of the behavior in the pullout state for various fiber types.

The coefficient D controls the tension-softening behavior of SFRC. By determining its value for representative fiber types under wide range of values of other parameters, it becomes possible to estimate the behavior of other fiber types.

4. COMPARISON WITH EXPERIMENTAL RESULTS

(1) Material constants

A set of uniaxial tension tests for SFRC have been done [9), 10)] to obtain the deformational behavior as described in Appendix A. The experiment was conducted by pulling out 32 fibers simultaneously. For the purpose of data fitting, the mean value of 32 fibers is assumed to represent the deformational behavior of one fiber.

Analysis of numerous test data reveals that the optimum values of empirical material constants a_d and D_0 are always nearly the same. Therefore, they are fixed as $a_d = 0.05$, $D_0 = 0.9$. It is also set that $U_0 = 1$mm.

The snubbing friction coefficient can be determined from the result of the pullout test for each fiber-matrix combination. For the present test, i.e., pullout of steel fiber from high strength mortar, $f = 1.0$. The initial elastic modulus of steel fiber is taken as $E_{f_0} = 2.0 \times 10^5 \mathrm{N/mm^2}$. As a rough estimate, the first trial value of the maximum shear force per unit length q_y can be approximated by the maximum measured pullout force from experimental data divided by the length of fiber. This material constant controls the maximum pullout force at the fiber end P^*. Shear stiffness k of the matrix of the interface zone is taken as $k = 0.20 \times 10^5 \mathrm{N/mm^2}$.

The value of the fiber end spring constant k_{end} may be approximated independently by considering the fiber end condition which depends on each fiber geometry for a straight fiber, a hooked fiber and an anchored fiber. It is assumed that there is no spring at the end of a straight fiber. From the observation, the value of fiber end spring constant for an anchored fiber should be larger than that for a hooked fiber.

Other empirical material constants can be estimated from experimental data. The analysis of available test data shows some knowledge about the influence of the material constants on the deformational behavior of fiber pullout as summarized in the following.

- a_e
  Material parameter a_e controls the displacement at the peak shear force. For larger value of a_e, the peak shear force occurs at a larger displacement. The peak shear force of a hooked fiber occurs at a larger displacement than that of an anchored fiber. Therefore, a_e for fitting the pullout force-displacement curve of a hooked fiber should be chosen so as to be larger than a_e for fitting that of an anchored fiber. The displacement at the peak shear force is about 1mm from the test data. [9), 10)]
- p_d
  Material parameter p_d controls the shape of the strain-softening curve. Larger value of p_d gives a steeper strain-softening curve. Because of the rupture of an anchored fiber, its strain-softening curve is steeper than those of a straight fiber and a hooked fiber. Consequently, the value of p_d for an anchored fiber is larger than those for a straight fiber and a hooked fiber.

The fitting of test data was accomplished by a trial-and-error approach.

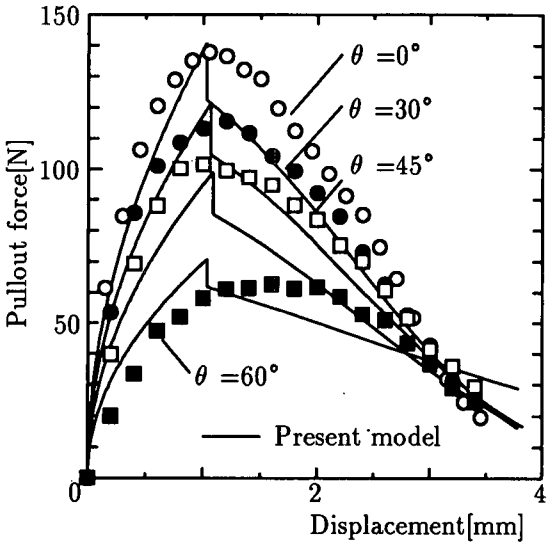

Fig. 5 Comparison with experimental results of fiber inclination effect

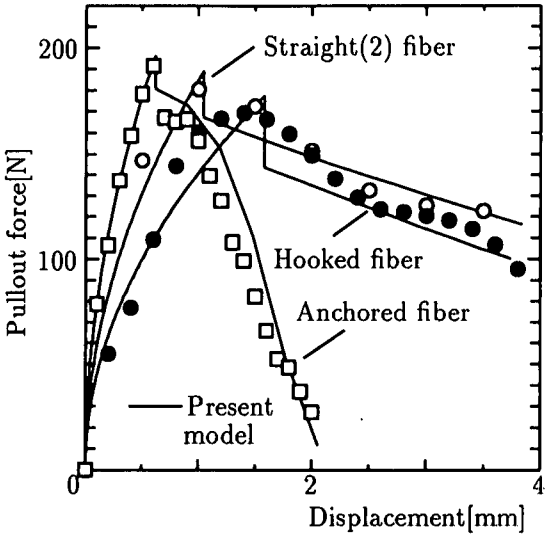

Fig. 6 Comparison with experimental results of fiber geometry effect

(2) Fiber inclination

To simulate the experimental results of inclined pullout test, the following parameters are used: L = 12.5mm, d = 0.55mm, k_{end} = 0.0N/mm. The optimum values of other material parameters are listed in **Table 1**.

The data fits of inclined fiber pullout test are shown in **Fig.5**. From the load-displacement curves, it is observed that the maximum pullout force is reduced for larger inclining angle. The maximum pullout force is 141N for θ = 0°, 119N for θ = 30°, 104N for θ = 45°, and 64N for θ = 60°. Compared with the maximum pullout force for θ = 0°, the reduction percentage becomes 16% for θ = 30°, 26% for θ = 45°, and 55% for θ = 60°.

The simulations include the elastic state, the full debonding at the peak, sudden failure, and the softening portion which is caused by the frictional pullout of fibers from the concrete matrix. The sharp drop of the pullout force at the peak observed in the simulation result may disappear in the case where the statistical variation of material properties is considered. It is confirmed that the numerical simulation using the present micromechanical model can express the deformational behavior of SFRC with the effect of fiber inclination satisfactorily.

(3) Fiber geometry

To simulate the experimental results of pullout test for the influence of fiber geometry, the following parameters are used: θ = 0°, L = 15mm. The optimum values of other material parameters are listed in **Table 2**.

The data fits of aligned fiber pullout test for different fiber geometrical shape (straight(2), hooked and anchored fibers) are shown in **Fig.6**. The displacement-pullout force relationship for straight(2) steel fiber starts with an elastic state, followed by a debonding state up to the maximum pullout force. After a sudden failure, a frictional fiber pull out state continues.

The deformational behavior of hooked steel fiber is summarized as follows. The full debonding phenomenon occurs around the maximum pullout force, followed by a sudden failure. Subsequently, a plastic deformation of the fiber hook occurs. In these two geometrical shapes of steel fiber, there is no fiber rupture.

The deformational behavior of anchored steel fiber is different from other types. It is observed that after achieving the maximum pullout force, sudden failure occurs, followed by a small plastic deformation of the fiber in a small fiber pullout displacement. Then, fiber rupture occurs.

Similarly to the previous simulation for the influence of fiber inclination, the sharp drop of the pullout force at the peak observed in this simulation result may also disappear in the case where the statistical variation of material properties is considered. From these experimental data fitting results, it is confirmed that the present model can describe the deformational behavior of steel fibers with various geometrical shapes.

Table 1 Optimum values of material parameters of pullout test for fiber inclination

Type of specimen	θ (deg)	q_y (N/mm)	p_d	a_e
Straight fiber(1)	0	12.5	2.7	0.018
	30	10.8	2.6	0.015
	45	8.8	2.5	0.012
	60	6.3	1.8	0.009

Table 2 Optimum values of material parameters of pullout test for fiber geometry

Type of specimen	d (mm)	q_y (N/mm)	k_{end} (N/mm)	p_d	a_e
Straight fiber(2)	0.60	14.0	0	1.0	0.024
Hooked fiber	0.60	13.0	20000	1.3	0.015
Anchored fiber	0.50	14.0	40000	5.5	0.063

5. CONCLUSION

A micromechanical fiber pullout model is proposed for SFRC. Comparing with the experimental results, it is confirmed that the present model is suitable to express the pullout mechanical behavior of SFRC under uniaxial tension.

The major findings of this study can be summarized as follows.

(1) The pullout behavior of steel fiber subjected to uniaxial tension is influenced by the fiber inclination. The maximum tensile pullout force is reduced for larger inclining angle.

(2) The pullout behavior of steel fiber subjected to uniaxial tension is also influenced by the geometrical shape of fiber. The pullout behavior of a straight fiber or a hooked fiber is more ductile than that of an anchored fiber. The increase of ductility is provided by the frictional resistance between the fiber surface and the concrete matrix.

(3) The pullout behavior of steel fiber described above can suitably be expressed by the present micromechanical fiber pullout model. Various stages of the fiber debonding and pullout process are clearly shown in the simulations of the aligned pullout test for several types of steel fibers and the inclined pullout test for various inclining angles.

ACKNOWLEDGMENT: The support of the Grant-in-Aid for Scientific Research (C) of the Ministry of Education to one of the authors is gratefully acknowledged.

APPENDIX A BRIEF SUMMARY OF THE PULLOUT EXPERIMENT[9),10)]

(1) Materials

The materials used are ordinary Portland cement, steel fibers, and river fine aggregate with maximum size of 5mm.

Four types of steel fibers are used in the experiment.

1) Straight(1) cut wire with indented surface (see **Fig.7(a)**). The equivalent diameter of the fiber is 0.55mm and the aspect ratio is 45. The length is 25mm and the tensile strength is 1000N/mm^2.
2) Straight(2) cut wire with indented surface (see **Fig.7(b)**). The equivalent diameter of the fiber is 0.60mm and the aspect ratio is 50. The length is 30mm and the tensile strength is larger than 1000N/mm^2.
3) Hooked cut wire with smooth surface (see **Fig.7(c)**). The equivalent diameter of the fiber is 0.60mm and the aspect ratio is 50. The length is 30mm and the tensile strength is larger than 1100N/mm^2.
4) Anchored stainless steel wire with a round block at both ends (see **Fig.7(d)**). The equivalent diameter of the fiber is 0.50mm and the aspect ratio is 60. The length is 30mm and the mean tensile strength is 1000N/mm^2.

In order to obtain homogeneous matrix in a specimen, coarse aggregates are not used. Furthermore, a superplasticizer (anion type agent) is used to improve the workability.

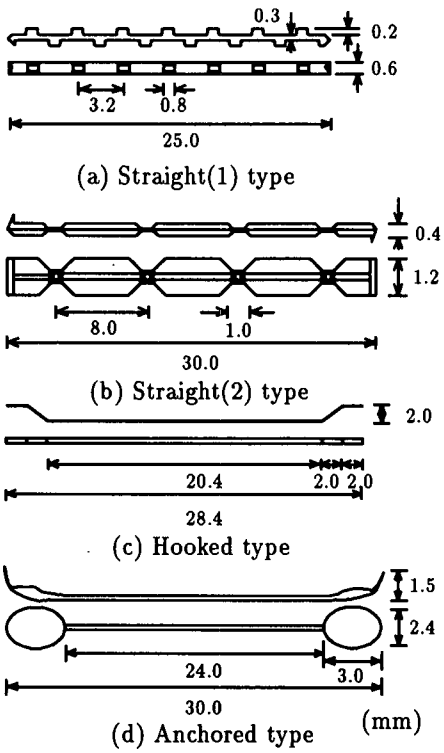

Fig. 7 Type of steel fiber

(2) Specimen and mix composition

Specimens are made from high strength mortar. The water-cement ratio is 0.3 and the sand-cement ratio is 1.0. Each specimen consists of two parts, i.e., upper block and lower block of the same size. It is assumed that crack has occurred at the discontinuous plane between two blocks. The size of the discontinuous plane is 100×100mm. The total height of the specimen is 300mm. Steel fibers are arranged to have a certain inclination angle to the discontinuous plane with the same embedment length in two blocks. The number of fibers is 32 (8 rows and 4 columns). Fibers are allocated in a grid position with longer spacing 20mm and shorter spacing 10mm.

(3) Loading method

The specimen is loaded at the age of 28days after curing in 20°C water. The average compressive strength of the age of 28days is 54.8N/mm^2. The load is applied to push down the lower block by the hydraulic universal testing machine with a loading rate of 0.25 N/s, while the upper block is supported. The pullout slip of fibers is measured by LVDTs at both sides of a specimen.

APPENDIX B NOTATION

A_f = cross-sectional area of fiber
a = debonded length
a_d, p_d = material parameters related to D
a_e = material parameter related to E_f
D = q_f/q_y
D_0 = initial value of D
d = diameter of fiber
E_f = effective elastic modulus of fiber
E_{f_0} = elastic modulus of fiber
f = snubbing friction coefficient
k = shear stiffness of interface zone
k_{end} = spring constant of spring at fiber end
L = fiber embedment length
L_f = frictional length of fiber
P^* = fiber pullout load
P_θ = maximum pullout load for inclined fiber
q = shear force per unit length of fiber
q_f = frictional shear force per unit length of fiber
q_y = maximum shear force per unit length of fiber
U_0 = a constant(= 1mm)
U^* = fiber end displacement
θ = fiber inclining angle
ω = interface parameter($\sqrt{k/(E_f A_f)}$)

REFERENCES

1) Nanakorn, P., Horii, H. and Matsuoka, S.: A fracture mechanics-based design method for SFRC tunnel linings, *J. Materials, Conc. Struct., Pavements*, No. 532/V-30, pp.221–233, 1996.
2) Cho, R. and Kobayashi, K.: Testing method for tensile strength of steel fiber reinforced concrete, *Concrete Journal, JCI*, Vol.17, No.9, pp.87–95, 1979.
3) Chern, J.C., Yang, H.J., and Chen, H.W.: Behavior of steel fiber reinforced concrete in multiaxial loading, *Materials Journal, ACI*, Vol.89, pp.32–40, 1992.
4) Banthia, N., Mindess, S. and Trottier, J.-F.: Impact resistance of steel fiber reinforced concrete, *Journal of Materials in Civil Engineering*, Vol.93, No.5, pp.472–486, 1996.
5) Sumitro, S. and Tsubaki, T.: Micromechanical constitutive relationship of steel fiber reinforced concrete, *Transactions of the JCI*, Vol 18, pp.159–166, 1996.
6) Sumitro, S. and Tsubaki, T.: Micromechanical constitutive relationship of steel fiber reinforced concrete with strain rate effect, *Proc. of the JCI*, Vol.19, pp.537–542, 1997.
7) Naaman, A.E. and Shah, S.P.: Pull-out mechanism in steel fiber-reinforced concrete, *J. of*

Struct. Div., Proc. of ASCE, Vol.102, No. ST8, pp.1537–1548, 1976.
8) Ouyang, C., Pacios, A. and Shah, S.P.: Pullout of inclined fibers from cementitious matrix, *Journal of Engineering Mechanics, ASCE*, Vol.120, No.12, pp.2641–2659, 1994.
9) Tsubaki, T., Sumitro, S. and Shoji, H.: Modeling of tensile and shear mechanical properties of steel fiber reinforced concrete, *Concrete Research and Technology*, Vol.8, No.1, pp.233–241, 1997.
10) Tsubaki, T. and Sumitro, S.: Effect of fiber type on the mechanical behavior of steel fiber reinforced concrete subjected to uniaxial tension, *Proc. of the Sixth East Asia-Pacific Conf. on Struct. Eng. & Constr.*, Vol.3, pp.1959–1964, 1998.
11) Nammur, G. and Naaman, A. E.: Bond stress model for fiber reinforced concrete based on bond stress-slip relationship, *Materials Journal, ACI*, Vol. 86, No.1, pp.45–57, 1989.
12) Gao, Y.C., Mai, Y.W. and Cotterell, B.: Fracture of fiber-reinforced materials, *Journal of Applied Mathematics and Physics* (ZAMP), Vol. 39, pp.550–572, 1988.
13) Stang, H., Li, Z. and Shah, S.P.: Pullout problem: stress versus fracture mechanical approach, *Journal of Engineering Mechanics*, Vol.116, No.10, pp.2136–2150, 1990.
14) Li, Z., Mobasher, B. and Shah, S.P.: Characterization of interfacial properties in fiber-reinforced cementitious composites, *J. Am. Ceram. Soc.*, Vol. 74, No.9, pp.2156–2164, 1991.
15) Li, V.C., Wang, Y and Backer S.: A micromechanical model of tension-softening and bridging toughening of short random fiber reinforced brittle matrix composites, *J. Mech. Phys. Solids*, Vol. 39, No.5, pp.607–625, 1991.

(Received March 18, 1997)

鋼繊維補強コンクリートの微視的構造を考慮した繊維引抜けモデル

Sunaryo SUMITRO ・ 椿　龍哉

一軸引張を受ける鋼繊維補強コンクリートの変形挙動を表現するための微視的構造を考慮した構成関係を示す．微視的な構成関係の特性はコンクリートと繊維の間の非線形界面領域によって表される．繊維と母材の剥離は応力基準に基づくとする．すなわち，剥離領域の伝播の条件は界面に作用するせん断応力により表される．本モデルは，界面領域のせん断剛性と強度，摩擦による付着応力，繊維端部の拘束条件，および繊維方向角の影響を考慮することができる．本モデルの有効性は数値計算結果と実験データの比較により確認できる．